Journal of Materials Chemistry B

Accepted Manuscript

ROYAL SOCIETY OF CHEMISTRY

www.rsc.org/materialsB

Journal of Materials Chemistry B

Journal of Materials Chemistry B

Dynamic Article Links ►

Cite this: DOI: 10.1039/c0xx00000x

www.rsc.org/xxxxxx

Paper

Luminescent magnetic hollow mesoporous silica nanotheranostics for camptothecin delivery and multimodal imaging

Swagatika Sahu,[a] Niharika Sinha,[b] Sujit K. Bhutia,[b] Megharay Majhi[c] and Sasmita Mohapatra[a]*

Received (in XXX, XXX) Xth XXXXXXXXX 20XX, Accepted Xth XXXXXXXXX 20XX
DOI: 10.1039/b000000x

The synthesis of a novel and specific nanoplatform for simultaneous anticancer drug delivery, fluorescence imaging and contrast agent in magnetic resonance imaging has been described. Hierarchical theranostic hollow magnetic mesoporous spherical particles with fluorescent carbon encapsulated within mesoporous framework have been prepared by hydrothermal carbonization approach. The particles show MR contrast behaviour by affecting the proton relaxation with transverse relaxivity (r_2) 150.03 $mM^{-1}S^{-1}$. These multifunctional fluorescent magnetic nanoparticles have been conjugated with hydrophobic drug camptothecin and a molecular marker folic acid using appropriate surface chemistry. The drug conjugated hybrid nanoparticles inhibit cell growth through induction of apoptosis as demonstrated in HeLa cells.

1. Introduction

The treatment of cancer could be greatly improved with early detection and diagnosis, targeted delivery of therapeutic agents, and efficient monitoring of the therapy.[1] Nanotechnology provides an opportunity to develop theranostic agent at nanoscale that has the combined advantages of sensitive in vivo imaging, ample drug storage and controlled drug release capability.[2-4] In past few years extensive effort has been devoted to the design of nanohybrid materials incorporating magnetic and luminescent functionalities into a single platform for biological applications such as magnetic resonance imaging (MRI) contrast, fluorescence imaging and drug delivery.[5-7] Among various hybrid composite materials, mesoporous silica based composites have attracted great interest because of low cytotoxicity, excellent chemical stability, the ease of surface modification, and large surface area which ensure facile adsorption as well as high loading of various therapeutic toxins.[8]

Luminescent carbon dot (CD) presents an attractive alternative to the conventional organic dyes or semiconductor quantum dots in bioimaging, because of their good biocompatibility, green synthesis and excellent luminescence properties.[9-12] Though within a short period, significant interest has been remunerated to explore CDs' potential in varieties of applications such as sensing,[13] biological labelling,[14] photo-catalysis[15] and optical-electronic devices,[16] only limited examples are available towards the theranostic application of CD where its fluorescent property can hand out the real time monitoring of the drug release efficacy. Recently, Chou et al. reported a facile method for the gram scale production of CD/mSiO_2-PEG which was used in controlled release of doxorubicin in HeLa cells.[17] Gajbhiye et al. synthesised a magnetic nanoparticle doped carbogenic nanocomposite for magnetic resonance and fluorescence multimodal imaging and demonstrated its efficiency in both in vitro and in vivo fluorescence as well as magnetic resonance imaging.[18]

On the other hand, Camptothecin (CPT), a plant alkaloid isolated from *camptotheca acuminate* shows significant antitumor activity in a broad spectrum of human malignancies. CPT can effectively inhibit the relaxation process of DNA related to replication and transcription by the stable combination with topoisomerase I and DNA.[19] Unfortunately, the clinical application of CPT is hampered by its poor pharmaceutical profile, with extreme aqueous insolubility, low stability of the lactone form at physiological pH,[20] and severe systemic toxicities.[21] As a consequence, a variety of nanomedicines including polymer drug conjugates,[22] micelles,[23] nanoparticles (NPs),[24] and vesicles[25] were developed for CPT delivery to decrease potent toxicities and improve its properties. However most of these carriers cannot congregate formulation requirements like controlled size with low dispersity, high loading efficiency, controlled drug release kinetics, sufficient aqueous stability, capability of staying nonaggregated in biological media and easy production from gram to kilogram scale, which are very much decisive for their clinical translation.[26] One important strategy to improve CPT delivery is specific targeting and appropriate conjugation of the drug through flexible surface chemistry. Active targeting of the drug through folate receptor is an emerging therapy strategy which enables the specific delivery of chemotherapeutic agents to aberrant tissues,

[a]*Department of Chemistry, National Institute of Technology, Rourkela, India-769008, E-mail: sasmitam@nitrkl.ac.in Fax:91-661-2462651; Tel: 91-661-2462661*
[b]*Department of Life Science, National Institute of Technology, Rourkela, India-769008*
[c]*Department of Radiology, Ispat General Hospital, Rourkela, India-769005*

thereby increasing their local efficacy while limiting their peripheral toxicity.[27] Recently, Zhang et. al.[28] have reported novel luminescent magnetic CdTe/ iron oxide nanoparticles with folate-conjugated tetrapeptide composites for tumor-targeted CPT delivery. Shi et al have developed a hyaluronic acid decorated mesoporous silica nanoparticles with carbon and silicon nanocrystals encapsulated with in frame work for active targeting of camptothecin through CD44 protein receptor.[29] Although these novel multifunctional nanoparticles possess reasonably good biocompatibility and growth inhibition properties, the possibility for long term slow release of Cd leading to cytotoxicity[30] and the low drug loading efficiency owing to the lack of robust drug conjugation chemistry limit their practical medical application. In this context, it is important to develop a stable biocompatible fluorescent magnetic carrier with ample loading efficiency as well as active targeting of camptothecin where the magnetic carrier labelled with highly luminescent carbon dot could be tracked to obtain imaging of migration and anchoring of the drug in vivo.

In the present paper, hollow mesoporous silica based luminescent magnetic hybrid nanoparticles by incorporating iron oxide nanoparticles as magnetic and carbon dot as the luminescent component have been developed. Hollow spheres have been demonstrated to show improved performance in drug delivery, because of a larger fraction of voids in their inner space which facilitates incorporation of large amount of drugs.[31,32] In this work the water soluble conjugate of CPT has been synthesized and coupled to the nanohybrid surface through robust chemistry using silane coupling agent. Furthermore, folic acid has also been conjugated to ensure the targeted specific delivery of the drug. After a series of physical characterizations like XRD, SQUID measurements, Raman, and TEM, the conjugation of the drug has been established through FTIR and XPS studies. The DLS and zeta potential studies over time ensure excellent stability of the nanoparticles in physiological medium. The in vitro cytotoxicity of the drug carrier as well as drug release profile has also been investigated. The intracellular uptake efficacy and the cell apoptosis was thoroughly investigated through fluorescent microscopy.

2. Experimental

2.1 Materials

Acetone, chloroform, diethyl ether, dichloromethane, ethanol, ethyl acetate, and triethyl amine were procured from Rankem, India. Benzyl ether, Cetyltrimethylammonium bromide (CTAB), camptothecin(CPT),Fe(acac)3,3-glycidoxypropyl trimethoxy silane (GTPS), oleic acid, oleylamine, tetraethyl orthosilicate (TEOS), diglycolic anhydride, diisopropylcarbodimide and 2,2'-(ethylenedioxy)-bis-(ethylamine) (EDBE) were purchased from Sigma Aldrich, USA. Dimethylaminopyridine (DMAP) and t-butanol were bought from Spectrochem Private Limited. Commercially available dichloromethane and toluene were purified by distillation over phosphorous pentoxide and sodium metal with benzophenol respectively. Prior to use, dimethylsulfoxide (DMSO) was vacuum distilled. All other reagents and solvents were used without further purification. Millipore water (18.2 MΩ cm) was used throughout the experiment.

2.2. Synthesis of γ-N-{2-[2-(2-aminoethoxy)ethoxy]ethyl} conjugated camptothecin (EDBE-CPT)

2.2.1. *Synthesis of mono-t-butylester of diglycolic acid (**1**)*

A solution of diglycolic anhydride (1 g, 9 mmol) and DMAP (1.05 g, 9 mmol) in dry t-butanol (8 mL) was stirred at reflux temperature for 18 h.[33] The solvent was removed under reduced pressure and the residue was dissolved in water. The aqueous solution was acidified to pH 2.5–3.0 with 1 N HCl and extracted with diethyl ether, dried over anhydrous Na_2SO_4 and concentrated under reduced pressure to give **1** (1.3 g, yield 79%). IR (KBr): 3468, 2986, 2922, 2846, 1739, 1636, 1398, 1370, 1303, 1246, 1140, 1054 cm^{-1}. ^{1}HNMR (400 MHz, $CDCl_3$): δ 8.74 (s, br, 1H), 4.26 (s, 2H), 4.13 (s, 2H), 1.49 (s, 9H). ^{13}C NMR (100 MHz, $CDCl_3$): δ 173.1, 169.9, 83.0, 69.3, 68.9, 28.0. MS (ESI): m/z (relative intensity) 213.1 ([M+Na], 100).

2.2.2. *Synthesis of camptothecin-20-monoester of mono-t-butylester of diglycolic acid (**2**) and diglycolicacid (**3**).*

A mixture of 1 (42 mg, 0.2 mmol), camptothecin (40 mg, 0.1 mmol), DMAP (27 mg, 0.2 mmol), and DIPC (0.03ml, 0.2 mmol) in anhydrous dichloromethane (6 ml) was stirred for 24 h at room temperature.[33] The reaction mixture was washed with water, then saturated sodium bicarbonate, 0.1 N HCl and again with water. The organic layer was dried over anhydrous $Na_2SO_4$and the solvent was removed under reduced pressure, recrystallization of the resultant solid from dichloromethane/ether gave 2(53 mg, yield 66 %). IR (KBr): 3395, 2923, 2846, 1742, 1717, 1653, 1619, 1558, 1502, 1460, 1432, 1418, 1399, 1368, 1275, 1253, 1194, 1139, 1057 cm^{-1}1HNMR (400 MHz, DMSO-d_6): δ 8.70 (s, br, 1H), 8.18-8.12 (m, 2H), 7.87(t, 1H), 7.72 (t, 1H), 7.13 (s, 1H), 5.52 (s, 2H), 5.31 (s, 1H), 4.60-4.55 (d, 2H), 4.43-4.39 (d, 2H), 2.17-2.13 (m, 2H), 1.40 (s, 9H), 0.94 (t, 3H). ^{13}C NMR (100 MHz, DMSO-d_6): δ 169.3, 168.9, 167.5, 157.2, 152.8, 148.3, 146.5, 145.6, 130.8, 129.3, 130.2, 129.0, 128.4, 128.2, 119.2, 95.3, 81.5, 76.8, 68.2, 67.4, 66.7, 50.7, 30.6, 28.1, 7.9. MS (ESI): m/z (relative intensity) 551 ([M+CH_3OH], 100).

A solution of compound **2** (80mg, 0.15 mmol) in dichloromethane (4 ml) and TFA (0.4 ml) was stirred at room temperature for 30 min. The solvent was removed under reduced pressure, and the resulting solid was recrystallized from dichloromethane/ether to yield **3**(51 mg, 81%). IR (KBr): 3337, 2970, 2913, 1740, 1678, 1650, 1618, 1575, 1522, 1457, 1432, 1395, 1360, 1323, 1256, 1197, 1170, 1138, 1060 cm^{-1}. ^{1}HNMR (400 MHz, DMSO-d6): δ 13.4 (s, 1H), 8.70 (s, 1H), 8.23-8.12 (m, 2H), 7.87(t, 1H), 7.72 (t, 1H), 7.14 (s, 1H), 5.52 (s, 2H), 5.30 (s, 1H), 4.62-4.58 (d, 2H), 4.44-4.40 (d, 2H), 2.17-2.14 (m, 2H), 0.99 (t, 3H). ^{13}C NMR (100 MHz, DMSO-d_6): δ 171.3, 169.4, 167.5, 157.0, 152.8, 148.3, 146.5, 145.6, 130.3, 130.8, 129.4, 129.0, 128.4, 128.2, 119.2, 95.4, 76.8, 67.7, 67.5, 66.7, 50.7, 30.6, 7.9. MS (ESI): m/z (relative intensity) 487 ([M+Na], 71)

2.2.3. *Synthesis of γ-N-{2-[2-(2-aminoethoxy)ethoxy] ethyl} conjugated camptothecin-20-monoester of diglycolic acid (CPT-diglycolic acid-EDBE) (**5**)*

Tert-butyl N-{2-[2-(2-aminoethoxy)ethoxy]ethyl}-carbamate was prepared according to our previously reported protocol. [34] A mixture of the carbamate (74 mg, 0.3 mmol), **3** (82 mg, 0.2 mmol), DMAP (54 mg, 0.4 mmol), and DIPC (0.06ml, 0.4 mmol) in anhydrous dichloromethane (10 ml) was stirred for 24 h at room temperature. The reaction mixture was washed with water, then saturated sodium bicarbonate, 0.1 N HCl and again with water. The organic layer was dried over anhydrous Na_2SO_4 and the solvent was removed under reduced pressure,

recrystallization of the resultant solid from dichloromethane/ether gave **4** (65 mg, 51%). IR (KBr): 3423, 3335, 3266, 3115, 2974, 2908, 1748, 1647, 1600, 1575, 1440, 1399, 1368, 1343, 1323, 1253, 1197, 1156, 1113, 1068, 1001 cm^{-1}.

^{1}HNMR (400 MHz, DMSO-d_6): δ 8.69 (s, 1H), 8.18-8.11 (m, 2H), 7.85(t, 1H), 7.71 (t, 1H), 7.35 (s, 1H), 6.77 (br s, 1H), 6.12 (br s, 1H), 5.43 (s, 2H), 5.28 (s, 1H), 4.61-4.57 (d, 2H), 4.44-4.39 (d, 2H), 3.49-3.44 (m, 8H), 3.49-3.43 (m, 2H), 3.06-3.04 (m, 2H), 1.90-1.85 (m, 2H), 1.33 (s, 9H), 0.99 (t, 3H).

^{13}C NMR (100 MHz, DMSO-d_6): δ 172.9, 157.3, 156.0, 154.4, 153.0, 150.5, 149.7, 148.4, 145.9, 130.9, 130.3, 129.5, 128.9, 128.4, 128.1, 119.5, 97.2, 78.1, 72.8, 70.6, 70.0, 69.9, 69.6, 68.2, 65.7, 66.7, 50.7, 39.0, 30.7, 28.7, 8.2. MS (ESI): m/z (relative intensity) 717 ([M+Na], 100)

A solution of compound **4** (96 mg, 0.15 mmol) in dichloromethane (5 ml) and TFA (0.5 ml) was stirred at room temperature for 30 min. The solvent was removed under reduced pressure, and the resulting solid was recrystallized from dichloromethane/ether to yield **5** (63 mg, 78%).

IR (KBr): 3426, 3273, 3109, 2963, 2913, 2851, 1743, 1675, 1650, 1597, 1580, 1502, 1482, 1435, 1399, 1345, 1317, 1273, 1259, 1197, 1156, 1133, 1068, 1032, 1001 cm^{-1}.

^{1}HNMR (400 MHz, DMSO-d6): ^{1}HNMR (400 MHz, DMSO-d_6): δ 8.69 (s, 1H), 8.18-8.11 (m, 2H), 7.85(t, 1H), 7.71 (t, 1H), 7.35 (s, 1H), 6.77 (br s, 1H), 6.12 (br s, 1H), 5.43 (s, 2H), 5.28 (s, 1H), 4.61-4.57 (d, 2H), 4.44-4.39 (d, 2H), 4.3-4.0 (br S), 3.59-3.54 (m, 2H), 3.4-3.35 (m. 2H), 1.89-1.85 (m. 2H), 0.9-0.86 (t, 3H). ^{13}C NMR (100 MHz, DMSO-d_6): δ 172.9, 159.0, 158.62, 157.31, 152.98, 150.47, 148.37, 145.94, 130.86, 130.26, 129.46, 128.95, 128.41, 128.12, 119.51, 97.22, 72.84, 69.83, 67.08, 65.71, 65.36, 50.68, 41.16, 30.75, 23.69, 8.20. MS (ESI): m/z (relative intensity) 595 ([M+1], 100).

2.3. Synthesis of luminescent magnetic mesoporous silica nanoparticle conjugated with folate and camptothecin

2.3.1. Synthesis of CD decorated magnetic mesoporous silica

Hydrophobic Fe_3O_4 nanoparticles were prepared by the method reported by Sun et al[35] and were coated with mesoporous silica using CTAB as a template.[36] Deposition of luminescent carbon dot (CD) on the surface of mesoporous silica coated magnetic particle (Fe_3O_4@m-SiO_2) was achieved by hydrothermal carbonization of orange juice in the template free channels of the mesoporous silica. In a typical procedure, dispersed Fe_3O_4@m-SiO_2 nanoparticles (200 mg in 10 ml ethanol) were mixed with 25ml of orange juice (absolutely pulp free) in 20 ml ethanol and then the mixture was transferred into an 80 ml Teflon-lined stainless-steel autoclave and was heated at constant temperature of 130°C for 150 min (1°C/min). After the reaction, the autoclave was cooled down naturally. The resulted luminescent magnetic nanocomposite (Fe_3O_4@m-SiO_2-CD) was magnetically separated and first washed thoroughly with dichloromethane followed by water to remove the water soluble adsorbed luminescent CDs.

2.3.2. Synthesis of folate and camptothecin conjugated CD decorated magnetic mesoporous silica

A mixture of 0.2 ml (0.88 mmol) 3-glycidoxypropyltrimethoxysilane and Fe_3O_4@m-SiO_2-CD particles (300 mg) in dry toluene (30 ml) was stirred and heated at reflux under dry nitrogen gas with triethylamine as a catalyst for 24 h. The functionalized particles were magnetically separated, washed extensively with acetone, and dried. Prior to synthesis of folate decorated Fe_3O_4@m-SiO_2-CD, amine functionalized folic acid is prepared using our previously reported procedure.[22] For conjugation, amine functionalized folic acid (FA-NH_2) (11 mg, 0.02 mmol) dissolved in DMSO was stirred overnight at 70º C with dispersed epoxide ended Fe_3O_4-mSiO_2-CD (100 mg) in presence of $ZnCl_2$ catalyst. Finally folate decorated luminescent particles were magnetically separated and washed with water (Fe_3O_4@m-SiO_2-CD-FA). For conjugation of CPT, in a 50 ml two necked round bottom flask, EDBE-glycolic acid-CPT (**5**) (54 mg, 0.1 mmol) and catalytic amount of $ZnCl_2$ were taken in 5 ml dry DMSO. To this solution 100 mg Fe_3O_4@m-SiO_2-CD-FA nanoparticle in 10 ml DMSO was added and allowed to stir at 70 °C for 20 h in nitrogen atmosphere. Then the particles were recovered using magnetic separator, washed thoroughly with millipore water and suspended in phosphate buffer (pH 7.4) and used for in vitro studies (Fe_3O_4@m-SiO_2-CD-FA-CPT) .

2.4. Stability and release of camptothecin (CPT)

In order to study the CPT release behaviour, 5 ml suspension of Fe_3O_4@m-SiO_2-CD-FA-CPT particles (1 $mgmL^{-1}$) was suspended in a solution containing 0.1 mg mL^{-1}cathepsin B and 10 ml of FBS. The solution pH was adjusted to 4, 5, 6 and 7.4 using 0.1 M HCl and NaOH. At specified time intervals, accumulated amount of drug released into the solution was quantified using a UV-vis spectrophotometer, λ_{max} (CPT) = 366 nm. The release profiles were plotted as the relative release percentages of CPT against time. The drug loading capacity and encapsulation efficiency were determined according to our previously reported protocol.[37]

2.5. Cytotoxicity

Human cervical carcinoma (HeLa) cells were obtained from the National Centre for Cell Sciences (Pune, India), cultivated in minimal essential medium (MEM) and Dulbecco's modified eagle medium (DMEM) respectively supplemented with 10% fetal calf serum, 100 units/mL penicillin, and 100 µg/mL streptomycin, 4mM l-glutamine under 5% CO_2 and 95% humidified atmosphere at 37°C. From 105 cells/ml cell suspension, 180 µL cell suspension was seeded at into each well of 96 wells tissue culture plates and incubated for 18 h followed by a addition of Fe_3O_4@m-SiO_2-CD, Fe_3O_4@m-SiO_2-CD-CPT nanoparticle, at concentrations 0.5 μgmL^{-1} to 50 μgmL^{-1} were incubated for 72 h at 37°C in a humidified incubator (HERA cell) maintained with 5% CO_2. The cell proliferation was estimated by MTT assay.

2.6. Intracellular uptake

Drug conjugated nanoparticles were incubated for 0, 30, 60 and 120 min with HeLa cells at a concentration of 5 μgmL^{-1}. Cells were then fixed with 4% paraformaldehyde after an incubation period of 15 min and stained with DAPI (1$mgmL^{-1}$) for 5 min at 37° C. Then cells were washed with PBS and examined under fluorescence microscopy.

2.9. DAPI staining for nuclear morphology

To study the nuclear morphology of the HeLa cells, DAPI staining was performed following the reported procedure. HeLa cells treated with PBS, 1, 5, 10 μg/ml of drug conjugated particles for 24 h. The cells were fixed with 3.7% formaldehyde for 15 min, permeabilized with 0.1% Triton X-100 and stained with 1 mg/ml DAPI for 5 min. The cells were then washed with PBS and examined under fluorescence microscopy.

2.9 Characterization

The phase formation and crystallographic state of the material were investigated by an Expert Pro Phillips X-ray diffractometer. Low angle powder X-ray diffraction (XRD) analysis was carried out with a Philips PW3040/00 diffractometer (operating at 40 kV and 30 mA), using a Cu Kα radiation (λ= 1.54˚A). The Raman spectrum of as-prepared samples was recorded at ambient temperature on Ranishawin Viarelex spectrometer (UK make). The morphology and microstructure were analyzed by scanning electron microscope (HITACHI COM-S-4200) and high resolution transmission electron microscopy (JEOL 3010, Japan) operated at 300 kV. The magnetic properties of Fe_3O_4@m-SiO_2 and Fe_3O_4@m-SiO_2-CD-FA-CPT composite nanoparticles were determined using a SQUID-VSM instrument (Evercool SQUID VSM DC Magnetometer) at 25.0 ± 0.5°C. The fluorescence emission spectra were performed on a Horiba Fluoromax 4 spectrophotometer at excitation energies ranging from 320 to 460 nm. Nitrogen adsorption/desorption isotherms were measured at a liquid nitrogen temperature (77 K) using a Quantachrome surface area analyser. The specific surface areas and total pore volume were calculated by the Brunauer–Emmett–Teller (BET) and BJH methods respectively. Mean hydrodynamic sizes were measured by laser light scattering using a particle size analyzer (Nano ZS 90, Malvern). Measurements were performed at 90° angle in 0.01 M phosphate buffer varying pH 4 to 9. The presence of surface functional group was investigated through FTIR spectra measured by a Thermo Nicolet Nexus FTIR model 870 spectrometer with the KBr pellet technique ranging from 400 to 4000 cm^{-1}. Surface composition of folate and CPT conjugated particles was investigated by analyzing XPS data using AlKα excitation source in ESCA-2000 Multilab apparatus (VG microtech). UV absorption measurements were carried out in Shimadzu 220V (E) UV-vis spectrophotometer to measure the CPT concentration (λ_{max}=366nm).

2.10. MR imaging

The relaxation time (T_2) and transverse relaxivity (r_2) of the nanoparticle were measured with varying iron concentration (0.015 – 0.075 mM) using a clinical MRI scanner (MAGNETOM Symphony, SIEMENS) at a magnetic field of 1.5 T. T_2-weighted images were obtained with a spin echo multisection pulse sequence having fixed repetition time (TR) of 4000 ms with various echo times (TE) ranging from 105 to 291 (105, 116, 128, 139, 151, 163, 174, 186, 198, 291). The spatial resolution parameters were as follows: field of view FOV = 300 ×300 mm^2, matrix = 358 × 358, slice thickness = 4.0 mm. The MRI signal intensity (SI) was measured using in-built software. T_2 values were obtained by plotting the SI of each sample over a range of TE values. T_2 relaxation times were then calculated by fitting a first-order exponential decay curve to the plot. The fitting equation can be expressed as:

$$SI = S_0 e^{-TE/T_2} + B$$

Where SI is the signal intensity, TE is the echo time, A is the amplitude, and B is the offset. The relaxivity value r_2 is determined from the slope of the linear plots of relaxation rate R_2 ($1/T_2$, s^{-1}) against Fe concentrations (mM).

$$R_2 = R_2^0 + r_2\,[Fe]$$

3. Results and Discussion

3.1 Synthesis

Scheme 1 represents our strategy for the formation of Fe_3O_4@m-SiO_2-CD hybrid nanoparticles. To synthesize Fe_3O_4embeded mesoporous silica nanoparticles through sol-gel method, the oleic acid coated magnetite crystals were made hydrophilic by coating CTAB as a secondary surfactant.[38] CTAB-stabilized nanocrystals acted as seeds for the formation of spherical mesoporous silica particles. CTAB served not only as the stabilizing secondary surfactant for the transfer of the nanocrystals to the aqueous phase but also the organic template for the formation of the mesoporous silica spheres. It was well established in our previous work that the major constituents orange juice such as sucrose, ascorbic acid and citric acid can act as efficient precursor for carbon dots.[12] The hydrogen bonding interaction between the surface silanol groups and constituents of orange juice facilitates the adsorption of precursors in the mesoporous channels which are converted to carbon dot upon hydrothermal treatment. Thus growth of carbon nanoparticles takes place within the porous frame work of mesoporous silica rather than outside. The overall Fe_3O_4@m-SiO_2-CD particles were functionalized with 3-glycidoxy- propyltrimethoxysilane to form epoxy ended Fe_3O_4@m-SiO_2-CD nanoparticles.

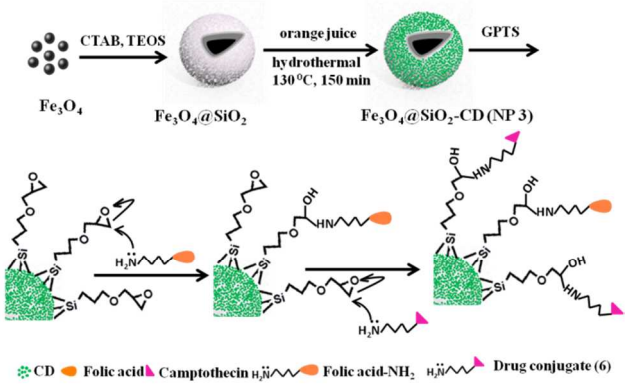

Scheme 1 Synthesis of fluorescent magnetic nanoparticles conjugated with CPT and folic acid

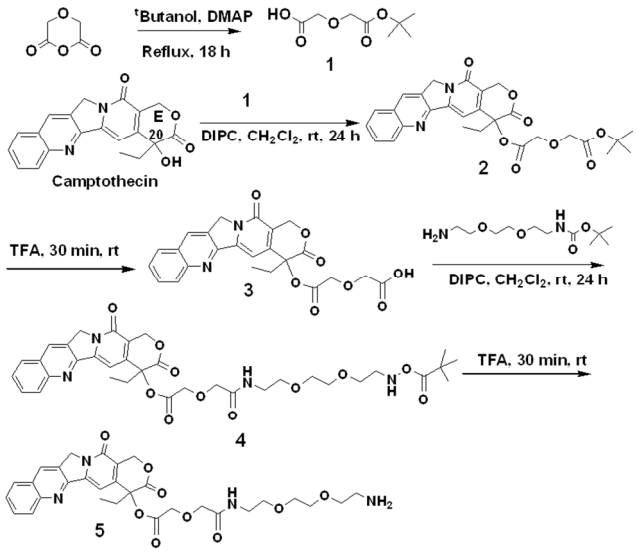

Scheme 2 Synthesis of camptothecin conjugated with EDBE

3.2 Conjugation of the drug

It has been reported that the solubility, tumor accumulation and circulatory retention of potent hydrophobic anticancer drug camptothecin dramatically increases by conjugating it with polyethylene glycol (PEG) dicarboxylic acid with the hindered tertiary alcohol at position 20 of ring E through a scissile ester bond.[39] We deemed to synthesize the water soluble form of camptothecin by coupling a small highly hydrophilic spacer (2,2'-(ethylenedioxy)-bis-(ethylamine) (EDBE) through a linker diglycolic acid (scheme 2). For this purpose diglycolic anhydride was first opened with tertiary butyl alcohol to give the protected ester acid **1**, followed by condensation with camptothecin in presence of DIPC and subsequent ester cleavage to give slightly water soluble derivative **3**. To this tert-butyl N-{2-[2-(2-aminoethoxy)ethoxy]ethyl}-carbamate (EDBE-Boc) has been coupled using carbodiimide to give **4** which after deprotection of Boc gives water soluble derivative **5**. Finally **5** has been coupled on Fe_3O_4@m-SiO_2-CD nanospheres through opening of epoxide in presence of catalytic amount of $ZnCl_2$. In a similar fashion, FA-NH_2 has also been coupled through epoxide opening in ordered to impart target specific delivery of the multifunctional particle (Scheme 1). We anticipate that such a strategy would have several advantages like 1) it will overcome the difficulties of functionalization with high molecular weight (> 1000Da) PEG,[40] 2) it can ensure a particle of controllable size which is not possible with high molecular weight polymers, 3) the drug cannot be escaped during the circulation before reaching the target site as it is strongly bound through covalent bond, 4) most importantly, it will release camptothecin in its active lactone form through a predictable hydrolysis of ester bond with in the tumor cell.

3.3 Structure and morphology

In the wide angle X-ray diffraction pattern of the Fe_3O_4@m-SiO_2-CD (Figure 1a), the diffraction peaks could be indexed to cubic spinel Fe_3O_4 having lattice parameter 8.3 Å. Apart from characteristic peaks of Fe_3O_4, the broad band at 18-22° can be assigned to amorphous silica shell (JCPDS No. 29-0085) and CD. In the low-angle XRD patterns (Figure1a, inset), two well-resolved diffraction peaks between 0.5 to 4.0° representing long range ordering of the mesoporous structure are observed. The peaks can be indexed to (100) and (110) reflections. These peaks have *d*-spacing ratios 1:√3 associated with ordered 2D hexagonal mesostructure (p6mm). The higher intensity of (110) reflection peak and the broadening of the peak in the composite compared to reported mesoporous silica may be attributed to the non-uniform distribution of matter in the unit cell and less structural ordering respectively due to carbonization under hydrothermal condition. In the wide angle XRD, the broad peak for carbon dot at 2θ=20-24° overlaps with amorphous mesoporous silica range, presence of CD cannot be distinguished from XRD pattern. However, appearance of two characteristic vibrations at 1363 and 1578 cm^{-1} for a defect band (D band) and a graphite band (G band) in the Raman spectrum (Figure 1b) confirms the deposition of CD on the silica coated magnetite. The G band is attributed to the vibration of sp^2-bonded carbon atoms in a 2D hexagonal lattice, while the D band is associated with vibrations of carbon atoms with dangling bonds in plane terminations of the disordered graphite. The I_D/I_G ratio was found to be 1.6, which is almost higher than that reported for bare CD. The relative high D-band intensity may be due to small particle size and the presence of abundant oxygen containing groups on the surface.[12] Furthermore, the distinct peaks at 680, 502 and 334 cm^{-1} correspond to magnetite core of the Fe_3O_4@m-SiO_2-CD nanoparticles. The TEM image (Figure 1c) of Fe_3O_4@m-SiO_2-CD particles show the formation of clear and spherical

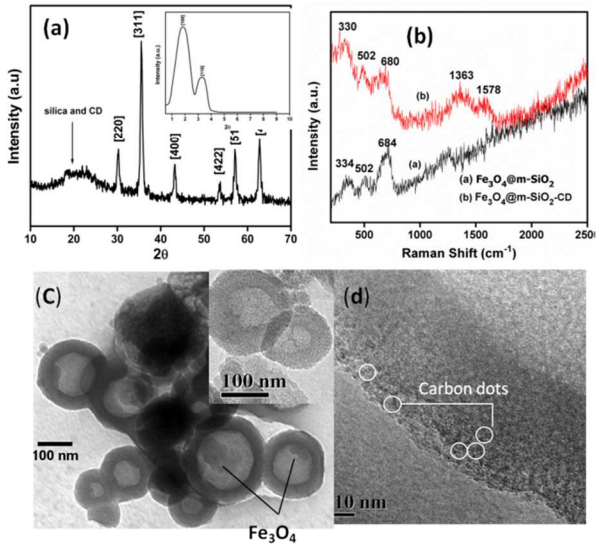

Figure 1(a) Wide angle X-ray diffraction pattern of Fe_3O_4@m-SiO_2-CD, low angle XRD (inset), (b) Raman spectra of Fe_3O_4@m-SiO_2 and Fe_3O_4@m-SiO_2-CD, (c) TEM images of Fe_3O_4@m-SiO_2-CD, (d) TEM image at higher magnification representing deposition of CDs in the mesopores.

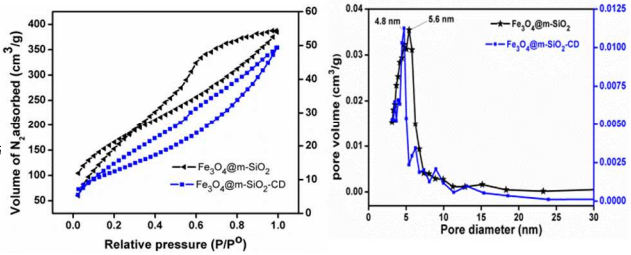

Figure 2 (a) N_2 adsorption-desorption isotherm and (b) pore size distribution of Fe_3O_4@m-SiO_2 before and after CD deposition

hollow silica spheres with a size range of 100-150 nm which is appropriate for drug and gene delivery.[41,42] The apparent aggregation of hollow spheres observed in TEM image might be due to TEM sample preparation and drying effect as observed in othercases.[43] Each silica sphere contains one or more magnetite nanocrystals embedded within its structure. The hollow structure arises because of trapping of ethyl acetate within the hydrophobic part of the mesophase during the sol-gel reaction[38] and remains structurally stable during the hydrothermal treatment. The porous nature of the silica is clear in the image at higher magnification (Fig 1c inset). The appearance of dark spotted ruffled surface in the high resolution image indicates the deposition of carbon dots in the mesoporous channels of the hollow silica sphere (Figure 1d).

The nitrogen adsorption desorption isotherm of the as prepared Fe_3O_4@ m-SiO_2 particles exhibits type IV isotherm with a hysteresis (Figure 2), which is a characteristics of mesoporous materials. The BET surface area was found to be 595 m^2/g. BJH pore size distribution determined from the desorption branch of the isotherm showed the formation of mesopores with maximum diameter centered at 5.6 nm and volume at 0.47 cc/g. However after carbonization the nature of the adsorption isotherm changes to type III due to formation of slit like pores. The BET surface area as well as pore diameter decreases to 135 m^2/g and 4.72 nm respectively after deposition of carbon dots on the inner surface. Though there is decrease in pore size and pore volume due to shrinkage of mesoporous wall during hydrothermal treatment and deposition of carbon dots still the surface area is reasonable for drug delivery applications.

3.4 Fluorescent, magnetic and relaxometric properties

The PL excitation spectrum recorded at λ_{em} of 400 nm shows three excitonic bands centered at 370, 350 and 338 nm. This behaviour indicates that there are at least three types of excitation energy trapped on the surface of the synthesized particle. When the sample is excited at 360 nm, there is a strong emission peak around 443 nm indicating a blue light emission (Figure 3a). The PL quantum yield was found to be 12.4% which is reasonably good (ESI for calculation). Unlike other semiconductor nanoparticles the photoluminescence in case of carbon dots is a combined effect of quantum confinement and surface defects that originate energy levels in between valence and conduction band that justifies light emission.[44] These electronic level distributions

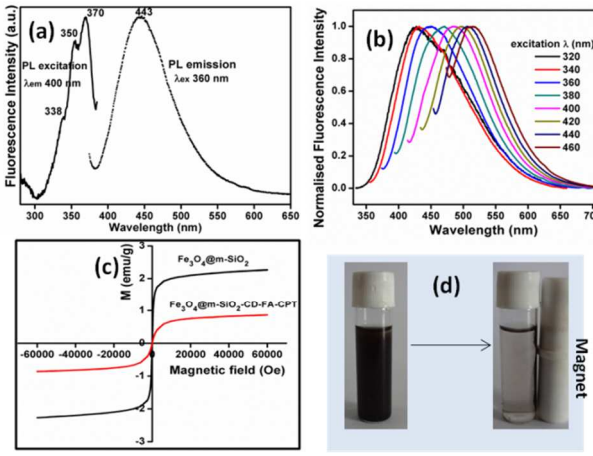

Figure 3 (a) Excitation-emission spectra, (b) wavelength dependent emission, (c) Room temperature magnetization behavior, (d) Interaction of Fe_3O_4@m-SiO_2-CD-FA-CPT particles with external magnetic field

allow radiative recombination of excitons.[45,46] Compared to bare CD prepared from orange juice as reported in our previous paper,[12] the emission spectrum of the Fe_3O_4@m-SiO_2-CD shows a narrower FWHM due to narrow size distribution upon growth of CD in a mesoporous template. The excitation dependent emission of Fe_3O_4@m-SiO_2-CD particles (Figure 3b) can be ascribed to surface states apart from reasons like free zig zag sites, aromatic conjugate structure, radiative recombinations as in case of carbon dots. Due to presence of several surface functional groups like C-OH, C-O-C, C=O, and C-H, a series of emissive traps between π and π^* states C=C are originated. When a certain excitation wavelength illuminates the CD a surface energy trap will dominate the emission. As the excitation wavelength changes, another corresponding surface state emissive trap will become dominant. In case of the hybrid particle the position of emission peak varied only slightly by altering the excitation indicating more uniform size distribution and less availability of free surface functional groups. However this excitation dependent emission gives rise to several visible consequences in fluorescence imaging and makes the material suitable as a bioimaging probe.

The field dependent magnetization for both the samples did not show hysteresis (Figure 3c), which represented their superparamagnetic characteristics desirable for their application in drug delivery. Figure 3d shows Fe_3O_4@m-SiO_2-CD-FA-CPT nanoparticles under external magnetic field. The saturation magnetisation (Ms) value for Fe_3O_4@m-SiO_2 was 2.2 emu g^{-1}, which is decreased to 0.9 emu g^{-1} on conjugation of folic acid and CPT. This decrease in saturation magnetization can be attributed to the combined effect of decrease in magnetic content as well as restriction in inter-particle magnetic coupling interaction due to surface modification by organic moiety. Furthermore, appreciably high deposition of CD on the surface of Fe_3O_4@m-SiO_2 is also responsible for this substantial reduction in magnetic saturation value. However, the saturation magnetisations value of the synthesized Fe_3O_4@m-SiO_2-CD-FA-CPT nanoconjugate fulfil the requirements for drug delivery, separation and MRI application.[47]

3.5 Conjugation of CPT and folic acid and surface composition

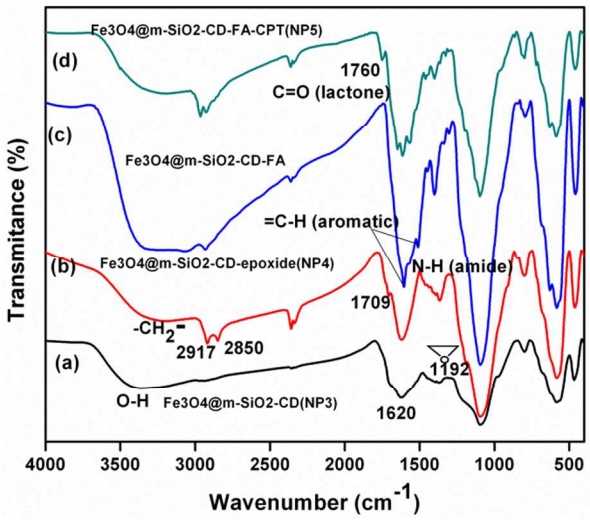

Figure 4 FTIR spectra of Fe_3O_4@m-SiO_2-CD-FA-CPT nanoparticles at various stages of synthesis

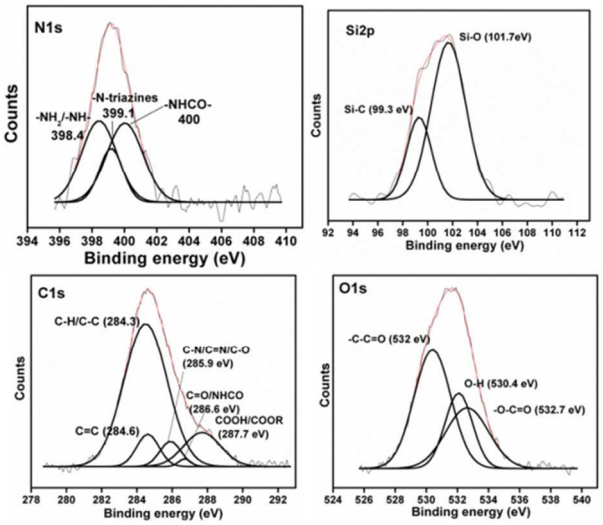

Figure 5 High resolution scan of Fe_3O_4@m-SiO_2-CD-FA-CPT corresponding to N1s, Si2p, C1s and O1s.

The FTIR spectra of Fe_3O_4@m-SiO_2-CD-FA-CPT at various stages of synthesis clearly establish the conjugation of the CPT and FA on the surface of the hybrid nanoparticles (Figure 4). Appearance of the broad bands centered at 3416 cm^{-1} in Fe_3O_4@m-SiO_2-CD suggest that a large number of OH groups and H_2O molecules exist on the surface, which not only play the major role in high aqueous stability but also provides enough scope for further functionalization of the particle. The broadness of the peak at 1620 cm^{-1} indicates the presence of functional groups like –COOH, -epoxy, carbonyl and hydroxyl groups on the surface as reported in case of hydrothermal synthesis of CD. The appearance of methylene peak at 2917 and 2850 cm^{-1} along with ring breathing frequency of epoxide at 1192 cm^{-1} and 1709 cm^{-1} corresponding formation of O=C-O-Si[48] in epoxy-functionalized particles indicates the surface modification with GTPS. The disappearance of epoxide ring breathing peak in Fe_3O_4@m-SiO_2-CD-FA-CPT shows the opening of the epoxide ring by the camptothecin conjugate **5** as presented in the scheme 1. Further, the appearance of C=O stretching at 1760 cm^{-1}correcsponding to lactones confirms the attachment of CPT on hybrid nanoparticles in its lactone form. Further insight into the surface composition was obtained from XPS (Figure 5). The peaks in the survey spectrum of Fe_3O_4@m-SiO_2-CD-FA-CPT at 100, 280-290, 400.3, 529-538, 705-730 eV correspond to binding energy of Si2p, C1s, N1s, O1s and Fe2p electrons with their atomic percentage 8.29, 59.37, 7.3 , 24.86, and 0.3 respectively (Fig S1, ESI). The high resolution scans of N1s region can be fitted into three peaks. The broad peak at 398.4 corresponds to –NH_2 in the folic acid, secondary amines in the linker and –NH_2 group of unreacted/physically adsorbed compound **5** and FA-NH_2. The peak appearing at 399.1eV is attributed to nitrogen present in the aromatic ring while the amide nitrogen appears at slightly higher energy 400.1 eV due to electron pulling effect of oxygen. Multiple Si2p photoemissions were observed corresponding to Si atoms bonded to C (Si−C, 99.3 eV) and Si atoms bonded to O (Si−O, 101.7 eV). The distinct high binding energy at about 287.7 and 286.6 eV were characteristic of the -COOH/-COOR and –C=O/NHCO group of CPT and folic acid which indicated their successful grafting onto the surface of nanoparticle. In addition to this the high resolution C1s shows emissions centered at 284.3, 284.6 and 285.9 corresponding to the C-C/C-H, C=C, C-N/C=N/C-O carbon. Furthermore, high resolution O1s photoemissions were also obtained corresponding to C-C=O, −OH (530.4, 532 eV) bond and a C−O−C=O bond (532.7 eV), which also confirmed the existence of folic acid and CPT. The surface composition was calculated from AAS, TG and elemental analysis. The TG analysis shows 4 % weightloss in the range 400° to 500°C which is attributed due to surface organic coating. Assuming the distribution of monodisperse hollow spheres of outer radius 76 nm and inner radius 41 nm, the number of chemically conjugated camptothecin and folic acid per hollow sphere have been calculated as 199 and 40. From specific surface area of Fe_3O_4@m-SiO_2-CD nanoparticles the number of hollow spheres per gram of sample has been estimated. The total iron content per gram of the sample has been calculated from AAS. Assuming uniform distribution of 5 nm Fe_3O_4 particles each hollow sphere receives 1.14 number of iron oxide nanoparticles (ESI for detail calculation).

The surface modification processes were further investigated by examining surface charge properties. The CPT-modified particles have positive zeta potential of +12.5 mV owing to the presence of surface –NH_2 group from folic acid. With decrease in pH up to 2.8 the zeta potential increases to 36.37 mV indicating the protonation of the free –NH_2 groups. At the same time with increase in pH the zeta potential becomes –ve due to opening of lactone ring of CPT giving rise to free acid (Fig S2, ESI). The hydrodynamic size of the nanoparticles after each step of the synthesis indicates the presence of stable non-aggregated particles which facilitates complete modification of the surface. In addition to this, HD size slightly increases after each modification indicating addition of one molecular layer after each step (Fig. S3, ESI). The HD size of the final conjugate (NP 5) is 122 nm. These functional nanoparticles were highly stable in aqueous medium as their HD size and PDI remain almost constant over a long time.

3.6 Camptothecin loading and release

The drug loading capacity of our fluorescent magnetic carrier is found to be 17.5%. Such high CPT loading is resulting from the high surface area of hollow mesoporous silica which facilitates more interior spaces and conjugation sites. It is noteworthy that such high drug loading capacity will allow small doses of Fe_3O_4@m-SiO_2-CD-FA-CPT circumventing the toxicity arising due to high doses of mesoporous silica.[49] The drug encapsulation efficiency of the carrier reached 87.5 %. The choice of cleavable ester bonds is perhaps the most promising strategy to release CPT at right place and right time through the enzymatic cleavage inside the lysosome. The imperative benefit of our fluorescent magnetic CPT-conjugate is that it prevents premature release of CPT before reaching the target. In absence of cathepsin B less than 19% of the drug was released after 20h incubation time which gradually increased to 52% by the end of 85h (Fig 6a). At the same time when the lysosomal condition was mimicked in presence of

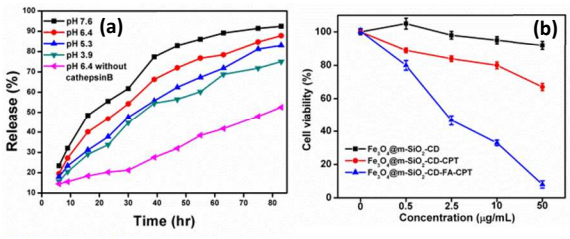

Figure 6 (a) Cumulative CPT releases from Fe_3O_4@m-SiO_2-CD-FA-CPT, (b) In vitro cell viability of HeLa with as prepared Fe_3O_4@m-SiO_2-CD and Fe_3O_4@m-SiO_2-CD-FA-CPT nanoparticles

enzyme cathepsin B, almost a burst release of 50% was observed in first 20h which slowly increased to 92% with 85 h incubation time at neutral pH. The drug release is higher at neutral pH and less acidic pH in accordance to other systems where drug is covalently attached to the carrier through ester linkage.[21] At pH 5.3, a burst release of 25% was observed after 10h, which gradually increased to 83% after 80h. Although the cumulative release of CPT is less than the same at alkaline pH, but the release behavior of our system at pH 4-5 is comparable or even better than the delivery systems already reported for camptothecin.[21-24] These results indicate that our Fe_3O_4@m-SiO_2-CD-FA-CPT nanoparticles can be used as a carrier for CPT without premature release of the drug in the blood vessel and also shows a sustained release pattern over a prolonged time inside the lysosomal compartment.

3.7 Cytotoxicity

CPT stabilises topoisomerase I-DNA covalent complex, hence prevents DNA relegation and subsequently induces DNA damage. As expected, the delivery of our system to HeLa cells leads to cell growth inhibition and finally cell death. To test the efficacy of CPT cleavage inside the target cells, HeLa cells were cultured with Fe_3O_4@m-SiO_2-CD, Fe_3O_4@m-SiO_2-CD-CPT and Fe_3O_4@m-SiO_2-CD-FA-CPT in a folate deficient medium. Nanoparticles deprived of CPT was found to be extremely noncytotoxic, where drug loaded particle (Fe_3O_4@m-SiO_2-CD-CPT) reduced cellular viability in a time and dose dependent fashion (Fig. 6b) establishing the ability of the cells to induce enzymatic cleavage of CPT. However, the proliferation of HeLa cells reduced dastrically in a dose dependent manner when incubated with Fe_3O_4@m-SiO_2-CD-FA-CPT. The IC_{50} value (the concentration at which cell growth is uninhibited by 50%) of our nanomedicine is found to be 2.1 μg/mL. This is attributed to the active uptake of nanoparticles in a folate receptor mediated endocytosis in the folate receptor over expressed HeLa cell that interfered with the cell proliferation.

3.8 In vitro Intracellular uptake, MRI and cell apoptosis

Cancer cell targeted drug delivery and optical imaging are demonstrated using our Fe_3O_4@m-SiO_2-CD-FA-CPT nanoparticles. Figure 7 illustrated fluorescence images of HeLa cells incubated with Fe_3O_4@m-SiO_2-CD-FA-CPT nanoparticles in a time dependent manner and DAPI was used as a nuclear contrast dye to appreciate localisation. The uptake of nanoparticles was clearly observed after 30 min. The green emission comes from carbon dots as already demonstrated in our previous paper and it was progressively increased in the cytoplasm. This suggests that nanoparticles are selectively targeted to the cells through the folate receptor mediated endocytosis and localized into the cytoplasm. The cytotoxic effect of Fe_3O_4@m-SiO_2-CD-FA-CPT was investigated by observing the nuclear fragmentation which is a trademark of apoptosis. With a dose dependent manner an increase in the formation of fragmented nuclei containing condensed nuclear material was observed in fluorescence microscopy after nuclear staining with DAPI (Figure 8).

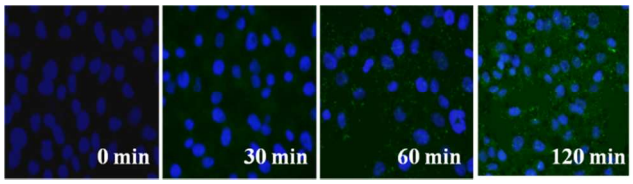

Figure 7 Representative fluorescence images of HeLa cells incubated with Fe_3O_4@m-SiO_2-CD-FA-CPT in different time intervals

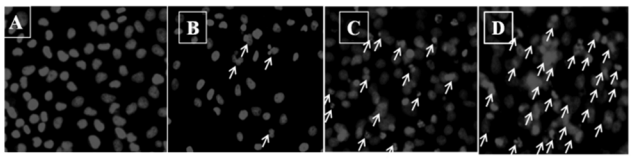

Figure 8 DAPI fluorescence (200X) images of HeLa cells incubated with (A)PBS, (B) 1, (C) 5, and (D) 10μg/ml Fe_3O_4@m-SiO_2-CD-FA-CPT for 24 h. The arrows represent apoptotic features such as nuclear condensation, fragmentation etc.

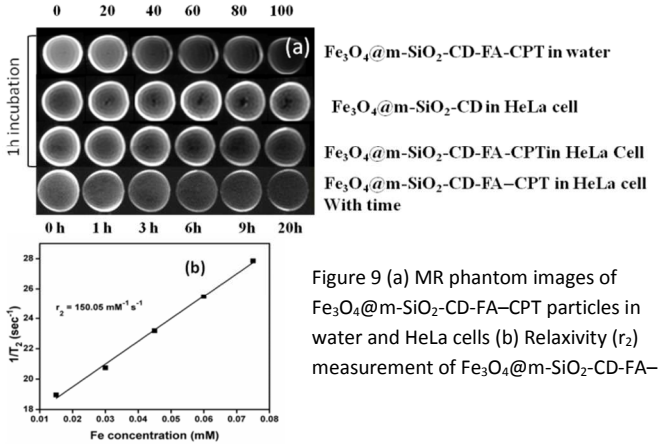

Figure 9 (a) MR phantom images of Fe_3O_4@m-SiO_2-CD-FA–CPT particles in water and HeLa cells (b) Relaxivity (r_2) measurement of Fe_3O_4@m-SiO_2-CD-FA–

As an initial investigation towards potential imaging functionality during chemotherapy, the visibility of nanocapsules was tested in water and HeLa cells by MRI. As shown in figure 9, with increasing concentration of Fe_3O_4@m-SiO_2-CD-FA-CPT in the phantom solution, the signal intensity decreased indicating that the magnetic hollow spheres have generated magnetic resonance contrast on transverse (T_2) proton relaxations times weighted sequence due to the dipolar interaction of magnetic moments between the nanoparticles and proton in the water.[50] The T_2 relaxation time was inversely proportional to the particle concentration as expected. The transverse relaxivity (r_2) of the drug conjugate is found to be 150.03 $mM^{-1}S^{-1}$ resulting in better negative contrast effect than commercially available dextran coated iron oxide such as feridex (r_2 =120 $mM^{-1}S^{-1}$), combidex (65 $mM^{-1}S^{-1}$), CLIO-tat (62 $mM^{-1}S^{-1}$).[51] Under T_2-weighted imaging mode, cells exposed to the magnetic nanocapsules of a concentration of 100μg/mL for 1h could be easily detected. In addition to this, maximizing the intake of nanoparticles through folate receptor mediated edocytosis in a folate-receptor overexpressed cancer cell would further enhance the contrast in MRI.[52]

4. Conclusion

Simple inexpensive hollow magnetic mesoporous silica based multimodal theranostic nanoagent bestowed with magnetic and receptor specific targeting, magnetic resonance and fluorescence imaging, high loading and controlled release of the anticancer drug camptothecin have been developed. These multifunctional nanoparticles are not only extremely stable in aqueous buffer but also possess appreciably good cytotoxicity through induction of apoptosis. Our surface engineering design promotes a reliable strategy for the administration of water insoluble drug camptothecin and at the same time the dual optical and magnetic property of the hollow spheres ensures fluorescence and MR-based imaging for the real-time monitoring of the treatment. This approach opens up a possibility for application of magnetic carbonaceous nanocomposite as a theranostic platform for cancer treatment and may be of particular interest in pharmaceutical industries.

Acknowledgements

The work is financially supported by BRNS, DAE, Govt. of India (Ref:2013/37C/8/BRNS/393). DST, New Delhi (SR/FIST/CS1-018/2010) is acknowledged for providing MS and Surface Area Analysis facility at NIT Rourkela.

References

1. M. K. Yu, J. Park and S. Jon, *Theranostics*, 2012, **2**, 3-44.
2. J. Huang, X. Zhong, L. Wang, L. Yang and H. Mao, *Theranostics*, 2012, **2**, 86-102.
3. H. S. Cho, Z. Dong, G. M. Pauletti, J. Zhang, H. Xu, H. Gu, L. Wang, R. C. Ewing, C. Huth, F. Wang and D. Shi, *ACS Nano*, 2010, **9**, 5398-5404.
4. H. Yoo, S. K. Moon, T. Hwang, Y. S. Kim, J. H. Kim, S. W. Choi and J. H. Kim, *Langmuir*, 2013, **29**, 5962-5967.
5. J. E. Lee, N. Lee, H. Kim, J. Kim, S. H. Choi, J. H. Kim, T. Kim, I. C. Song, S. P. Park, W. K. Moon and T. Hyeon, *J. Am. Chem. Soc*., 2010, **132**, 552–557.
6. J. Fang, M. Saunders, Y. Guo, G. Lu, C. L. Raston and K. S. Iyer, *Chem. Comm.*, 2010, **46**, 3074–3076.
7. D. Shi, H. S. Cho, Y. Chen, H. Xu, H. Gu, J. W. Wang, G. Liu, C. Huth, L. Wang, R. C. Ewing, S. Budko, G. M. Pauletti and Z. Dong, *Adv. Mater*., 2009, **21**, 2170–2173.
8. J. E. Lee, N. Lee, T. Kim, J. Kim and T. Hyeon, *Acc. Chem. Res*., 2011, **44**, 893-902.'
9. S. T. Yang, L. Cao, P. G. Luo, F. Lu, X. Wang, H. Wang, M. J. Meziani, Y. Liu, G. Qi and Y-Ping Sun, *J. Am. Chem. Soc.,* 2009, **131**, 11308–11309.
10. X. Zhai, P. Zhang, C. Liu, T. Bai, W. Li, L. Dai and W. Liu, *Chem. Commun.,* 2012, **48**, 7955–7957
11. Y. Yang, J. Cui, M. Zheng, C. Hu, S. Tan, Y. Xiao, Q.Yang and Y. Liu, *Chem. Commun.,* 2012, **48**, 380–382.
12. S. Sahu, B. Behera, T. K. Maiti and S. Mohapatra, *Chem. Commun.*, 2012, **48**, 8835-8837.
13. C. Yu, X. Li, F. Zeng, F. Zheng and S. Wu, Chem. Commun., 2013, **49**, 403-405.
14. Y. Yang, J. Cui, M. Zheng, C. Hu, S. Tan, Y. Xiao, Q. Yanga and Y. Liu, *Chem. Commun*., 2012, **48**, 380–382.
15. L. Cao, S. Sahu, P. Anilkumar, C. E. Bunker, J. Xu, K. A. S. Fernando, P. Wang, E. A. Guliants, K. N. Tackett, and Y-P Sun, *J. Am. Chem. Soc.* **2011**, 133, 4754–4757
16. S. Zhu, Q. Meng, L. Wang, J. Zhang, Y. Song, H. Jin, K. Zhang, H. Sun, H. Wang, B. Yang, *Angew. Chem. Int. Ed*. 2013, **52**, 3953 –3957.
17. C. Lai, Y. H. Hsiao, Y. K. Peng and P.T. Chou, *J Mat. Chem.*, 2012, **22**, 14403-14409.
18. S. Srivastava, R. Aswasthi, D. Tripathi, M. K. Rai, A. Agarwal, V. Agrawal, N. S. Gaibhiye and R. K. Gupta, *Small*, 2012, **8**, 1099-1109.
19. V. J. Venditto and E. E. Simanek, *Mol. Pharm*., 2010, **7**, 307–349.
20. Z. Mi, andT. G. Burke, *Biochemistry*, 1994, **33**, 10325–10336.
21. P. Botella, I. Abasolo, Y. Fernández, C. Muniesa, S. Miranda, M. Quesada, J. Ruiz, S. Schwartz Jr and A. Corma, *J Controlled Release,* 2011, **156**, 246–257.
22. N. Vijayalakshmi, A. Ray, A. Malugin and H. Ghandehari, *Bioconjugate Chem.,* 2010, **21**, 1804–1810
23. S. M. Page, M. Martorella, S. Parelkar, I. Kosif and T. Emrick, *Mol. Pharmaceutics,* 2013, **10**, 2684–2692.
24. K. J. Chen, L. Tang, M. A. Garcia, H. Wang, H. Lu, W. Y. Lin, S. Hou, Q. Yin, C. K. F. Shen, J. Cheng and H. R. Tseng, *Biomaterials,* 2012, **33**, 1162-1169.
25. P. S. Pramod, K. Takamura, S. Chaphekar, N. Balasubramanian and M. Jayakannan, *Biomacromolecules*, 2012, **13**, 3627−3640.
26. L. Tang, T. M. Fan, L. B. Borst and J. Cheng, *ACS Nano*, 2012, **6**, 3954-3966.
27. B. Stella, S. Arpicco, M. T. Peracchia, D. Desma¨ele, J. Hoebeke, M. Renoir, ˇ J. D angelo, L. Cattel and P. Couveur, *J. Pharm. Sci.*2000, **11,** 1452-1464.
28. J. M. Shen, X. M. Guan, X. Y. Liu, J. F. Lan, T. Cheng and H. X. Zhang, *Bioconjugate Chem.,* 2012, **23**, 1010−1021.
29. Q. He, M. Ma, C. Wei and J. Shi, *Biomaterials,* 2012, **33**, 4392-4402.
30. A. M. Derfus, W. C. W. Chan and S. N. Bhatia, *Nano Lett.,* 2004, **4**, 11-18.
31. W. Zhao, H. Chen, Y. Li, L. Li, M. Lang and J. Shi. *Adv. Funct. Mater.* 2008, 18, 2780–2788.
32. Y. Chen, H. Chen, D. Zeng, Y. Tian, F. Chen, J. Feng and J. Shi, *ACS Nano*, 2010, 4, 6001-6013.
33. R. B. Greenwald, A. Pendri, C. D. Conover, C. Lee, Y. H. Choe, C. Gilbert, A. Martinez, J. Xia, D. Wu and M. Hsue, *Bioorg. & Med. Chem.* 1998, **6**, 551-562.
34. S. Mohapatra, S. K. Mallick, T. K. Maiti, S. K. Ghosh and P. Pramanik, *Nanotechnology*, 2007**, 18**, 385102-11.
35. S. Sun and H. Zeng, *J. Am. Chem. Soc.,* 2002, **124**, 8201-8205.
36. S. Sahu and S. Mohapatra, *Dalton Trans*., 2013, **42**, 2224–2231.
37. S. Mohapatra, S. R. Rout, S. Maiti, T. K. Maiti and A. B. Panda, *J. Mat. Chem.*, 2011, **21**, 9185-9193.
38. J. Kim, J. E. Lee, J. Lee, J. H. Yu, B. C. Kim, K. An, Y. Hwang, C. H. Shin, J. G. Park, J. Kim and T. Hyeon, *J. Am. Chem. Soc.,* 2006, **128**, 688-689.
39. A. H. Lu, W. C. Li, W. Schmidt, W. Kiefer and F. Schüdt, *Carbon*, 2004, **42**, 2939-2946.

40. R. B. Greenwald, A. Pendri, C. Conover, C. Gilbert, R. Yang and J. Xia, *J med chem.,* 1996, **39**, 1938-1940.
41. Y. Zhu, Y. Fang and S. Kaskel, *J. Phys. Chem. C,* 2010, **114**, 16382–16388.
42. Y. Zhu, W. Meng, H. Gao and N. Hanagata, *J. Phys. Chem. C,* 2011, **11**, 13630–13636.
43. Z. Ya Ma, D. Dosev, M. Nichkova, S. J. Gee, B. D. Hammockb and I. M. Kennedy, *J. Mater. Chem*., 2009, 19, 4695–4700.
44. Nanomaterials: Chapter 10: *Carbon and Silicon Fluorescent Nanomaterials*, Page 237, ISBN 978-953-307-913-4
45. H. Peng and J. Trans-Sejdic, Chem. Mater, 2009, 21, 5563-5565.
46. H. Zhu, X. Wang, Y. Li, Z. Wang, F. Yanga and X. Yang, *Chem. Commun*, 2009, 34, 5118-5120.
47. J. Kim, H. S. Kim, N. Lee, T. Kim, H. Kim, T. Yu, I. C. Song, W. K. Moon and T. Hyeon, *Angew. Chem. Int. Ed.,* 2008, **47**, 8438 –8441.
48. H. Gaspar, C. Pereira, S. L. H. Rebelo, M. F. R. Pereira, J. L. Figueiredo and C. Freire, *Carbon,* 2011, **49**, 3441-3453.
49. S. P. Hudson, R. F. Padera, R. Langer and D. S. Kohane, *Biomaterials,* 2008, **29**, 4045-4055.
50. C. Sun, C.Fang, Z. Stephen, O. Veiseh, S.Hansen, D. Lee, R. G. Ellenbogen, J. Olson, M. Q. Zhang, *Nanomedicine* **2008**, *3*, 495–505.
51. H. B. Na, I. C. Song and T. Hyeon, *Adv. Mater.,* 2009, **21**, 2133–2148.
52. H. Yoo, S. K. Moon, T. Hwang, Y. S. Kim, J. H. Kim, S. W. Choi and J. H. Kim, *Langmuir,* 2013, **29**, 5962-5967.